Article:
Henthorn, S., O'Farrell, T., Anbiyaei, M.R. et al. (2023) Concurrent multiband direct RF sampling receivers. IEEE Transactions on Wireless Communications, 22 (1). pp. 550-562. ISSN: 1536-1276

https://doi.org/10.1109/twc.2022.3196279

Concurrent Multiband Direct RF Sampling Receivers

Stephen Henthorn, Timothy O'Farrell, *Senior Member, IEEE,* Mohammad Reza Anbiyaei, and Kenneth Lee Ford, *Senior Member, IEEE*

***Abstract*—Direct radio frequency (RF) sampling receivers are investigated for use in concurrent multiband reception for mobile broadband (MBB) applications. The recent proliferation of different frequency bands and standards in wireless communications has allowed large increases in mobility and throughput, but the number of receivers in a device is limited by physical space and power consumption. Software Defined Radio (SDR) is increasingly being explored to reduce the number of analog RF components required. This paper examines the use of direct RF digitization, allowing tunable and concurrent reception of multiple bands with a single RF front-end. Full mathematical models of both Nyquist and subband sampling receivers are presented and used to investigate a quadband LTE receiver, which is modeled in Simulink and implemented in a hardware-in-the-loop (HWIL) testbed. Individual bands are simulated to have at worst -95dBm sensitivity for 16-QAM with Nyquist sampling and -83dBm with subband sampling. Desensitization of the receivers due to multiband processing is evaluated theoretically and experimentally, showing a maximum of 3dB degradation, which is within the LTE standard for adjacent band interference.**

***Index Terms*—Software defined radio, direct RF sampling, subband sampling, multiband receiver, concurrent receiver**

I. Introduction

THE number of standards used in mobile communications is increasing, with different standards focussing on providing data throughput in different scenarios. This includes IEEE802.11 standards for high throughput data over local area networks, Bluetooth for low throughput over very short distances, the 3GPP standards for high mobility and throughput and many more. Further, to maintain back-compatibility with older networks, devices often need to operate with legacy standards of each type. Many of these standards also use multiple frequency bands, with the potential to increase total throughputs to devices through aggregation across these bands [1].

While this approach has allowed rapid expansion in the throughput and applications of mobile devices, the requirement for each band to have its own complete radio places strain on the physical space available inside devices, increases the power consumption thereby shortening the battery life of devices, and increases the cost of each device. There are several approaches to reducing this by switching between different bands [2], or by having single tunable RF front-ends [3]. However these do not allow the concurrent reception across multiple bands required for non-contiguous carrier aggregation (CA) or concurrent multistandard operation.

As such, new solutions for multiband and multistandard radios are being explored [4]. Dual-band non-contiguous CA has been performed with two separate reconfigurable RF front-ends [5], but reducing the component count further usually requires complex multiband devices, such as low noise amplifiers (LNA) and filters [6]–[9]. Alternatively, novel downconversion techniques such as using six-port correlators, harmonic recombination, or subsampling downconverters have been investigated [10]–[12].

An alternative approach is to leverage Mitola's vision of software defined radio (SDR) through direct RF sampling [13]. In the limit, a received signal is digitized by an analog to digital converter (ADC) as close to the antenna as possible and digital resources can be allocated dynamically to perform filtering, downconversion and baseband processing, allowing implementation of a flexible receiver capable of processing any number of different signals of any standard simultaneously. In practice some kind of RF front-end is still required to provide amplification and filtering of unwanted signals. This also offers potential for a reduction in receiver size by reducing the number of RF components required, especially mixers; and replacing multiple baseband ADCs with a single RF ADC, which may sample at Nyquist or subband rates. The subband case achieves the most reduction in space and power consumption, whereas the Nyquist case offers the most flexibility and more reliable transmission. This approach has previously been implemented using subsampling ADCs to receive two signals simultaneously [14], [15]. [14] uses bandpass filters within the ADC to suppress intermodulation products, allowing concurrent reception of 5 MHz bandwidth signals at 2.12 GHz and 2.4 GHz with a 400 MSample/s sampling rate. [15] focuses on the design of a tunable multiband filter embedded within the ADC, enabling concurrent reception of two global navigation satellite system (GNSS) signals in the 1.2 GHz and 1.57 GHz bands. However, in neither case is the system performance explored or the mathematical principles underpinning operation investigated.

This paper aims to contribute to the emerging field of concurrent multiband SDR receivers in three important ways. First, it will present the first full mathematical analysis of the performance of direct RF sampling receivers, giving a simple closed-form solution to inform design choices. Second, it will discuss at length multiband concurrent Nyquist direct

S. Henthorn, T. O'Farrell and K. L. Ford are with the Department of Electronic and Electrical Engineering, University of Sheffield, Sheffield, UK e-mail: t.ofarrell@sheffield.ac.uk

M. R. Anbiyaei is with the Department of Engineering, Al-Zahra University, Tehran, Iran

Manuscript received...

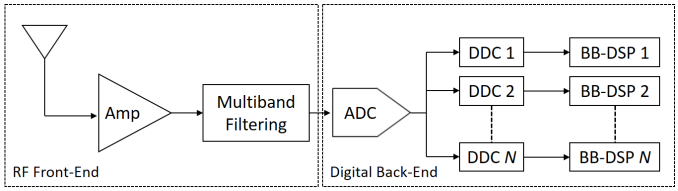

Fig. 1. Single-chain concurrent multiband tunable receiver concept

RF sampling receivers. ADC technology has now developed to the point where commercially available devices have RF bandwidths greater that 6 GHz and sampling rates greater than 12 GSample/s, allowing them to cover the whole sub-6 GHz radio spectrum [16]. As such Nyquist direct RF sampling receivers are increasingly feasible and should be investigated fully as well as subband schemes. Finally, this paper will design, simulate and implement a hardware-in-the-loop (HWIL) testbed for a quadband direct RF sampling receiver capable of concurrently receiving four 20 MHz LTE signals in different bands simultaneously, and measure the system performance. This will be performed with both Nyquist and subsampling ADCs, building on previous work from this group on HWIL triband receivers [17], [18]. While previous work has published initial results on dual- and tri-band receivers, this paper presents the first in-depth set of measured results for a concurrent quadband Nyquist direct RF-sampling receiver as well as the new mathematical framework for both Nyquist and subband direct sampling.

In Section II, the concept of the multiband multistandard receiver will be introduced and discussed in depth, with advantages and limitations discussed. Mathematical analysis of the theoretical performance of such a receiver will then be discussed in Section III, for both Nyquist and subsampling cases, focussing on the effect of desensitization of the ADC. The full design process for a quadband single-RF chain receiver of this kind will then be discussed in Section IV, along with modelling of its performance in Simulink in Section V. The receiver is then implemented in both a conducted and an over-the-air (OTA) hardware-in-the-loop (HWIL) testbed in Section VI, and key system performance indicators explored, in particular the constellation error vector magnitude (EVM) and block error rate (BLER) of LTE downlink waveforms under a variety of reception conditions.

II. Single-Chain Tunable Multiband Receivers

A diagram for the generic proposed receiver is shown in Fig. 1. The key element is the digitization of received signals as near to the antenna as possible in order to remove the majority of RF components. By using digital downconverters directly at RF, rather than at some downconverted IF, digital resources can be assigned dynamically to allow K different frequency bands to be concurrently mixed to baseband (BB). The number of bands is limited only by the resources available at the receiver. Further, the frequency of the digital local oscillators can be altered, making the digital back-end of the receiver fully tunable. The resources for baseband digital signal processing (BB-DSP), such as fast Fourier transforms (FFTs) for orthogonal frequency division multiplexing (OFDM), can also be allocated dynamically, allowing multistandard operation across all K bands.

The range of frequencies over which the digital back-end is able to operate is largely determined by the ADC, in particular its analog bandwidth and sampling rate. Nyquist's sampling theorem states that to preserve all information in a signal, $f_s \geq 2f_{max}$, where f_s is the sampling rate and f_{max} is the maximum frequency of the signal. As such, to cover the full sub-6GHz range of frequencies, an ADC capable of 12 GSample/s would be required. Recent advances in both semiconductor design and the use of time interleaving, where large arrays of sub-ADCs are run in parallel, have allowed sampling rates to reach up to 90 GSample/s [19]. Higher sampling rates tend to lead to either greater power consumption or component count. Further, the sample rate must be matched by at least the first DDC, leading to high demands in signal processing.

To minimise these issues, subband sampling techniques can be used [20]. By sampling significantly below the Nyquist frequency, image signals are created at lower frequencies which can then be digitally downconverted as before. Again, the ADC must respond to the whole desired RF bandwidth. The sampling frequency must be chosen carefully to avoid image signals overlapping with each other and causing loss of data. As no closed form solutions are available, a range of numerical algorithms exist for finding feasible sampling frequencies for a given set of signal bandwidths and carrier frequencies, usually with the aim of obtaining the minimum possible sampling rate [21]–[25]. Also, in the subband case, not all combinations of desired frequency bands can be supported. While co-prime subsampling has also been investigated for multiband data acquisition, this requires multiple ADCs [26], [27].

In both sampling cases, but especially when using subband sampling, the existence of image frequencies which would pass through digital filtering requires rejection of these frequencies in the RF front-end. As such, the quality of the channelisation filters is important. Note that strong stopband rejection and tunability are conflicting priorities, which are traded-off in today's front-end designs.

Amplification is also required to improve the sensitivity of the receiver. The precise configuration of amplification and filtering stages is flexible and may depend on the components used and application. The final stage of the RF front-end is the antenna. This could be wideband across all bands of interest, or multiband and possibly tunable. The latter has advantage in effectively acting as a first-stage filter to aid image rejection and reduce out-of-band noise.

As such, with careful design of the RF front-end, choice of ADC and allocation of digital resources, this general receiver configuration is capable of concurrent reconfigurable tunable reception. Its key disadvantage, however, is that the use of a single ADC for all bands can lead to desensitization where one desired signal has significantly lower power than the others. This is akin to the well-known near-far problem in uplink mobile communications [28]. The precise effects of this will be explored in the following sections, including analysis of quantisation noise, modelling of the receiver in Simulink and

experimental implementation in a HWIL testbed.

III. Noise in Multiband Directly Digitizing Receivers

Noise processes in SDR receivers are well studied and understood [29], [30]. However, the standard analysis contains many assumptions, which do not apply to multiband concurrent receivers. This section will derive an analysis to aid engagement with the key differences between conventional and multiband receivers, and allow reasonable estimation of expected performance. The case of Nyquist sampling at the ADC will be examined first, followed by subsampling.

A. Nyquist Sampling

The noise power in the signal bandwidth of any directly digitizing receiver has two key components: the digital noise, which is introduced by the ADC due to quantisation and jitter; and the RF noise, which is present at the input to the ADC but may be compounded through subsampling effects. Examining the RF noise first, in the Nyquist case this is entirely determined by the RF front-end design and the noise temperature T of the receiver. Taking signal band n with bandwidth B_n, over which the RF front-end has gain G_n and noise factor (NF) F_n, the noise power at the input to the ADC within that band is

$$N_{RF_{Nyq_n}} = k_B T B_n G_n F_n \tag{1}$$

where k_B is Boltzmann's constant. This represents the in-band noise power at the receiver input, $k_B T B_n$, being amplified and added to by the receiver's RF front-end. That is, the term in $G_n F_n$ accounts for the first and second stage amplifier gains G_{LNA_1} and G_{LNA_2}, and noise factors F_{LNA_1} and F_{LNA_2}, respectively, as well as the losses of the splitter/combiner and SAW filter. This gives a noise power for each individual band, allowing the performance of each band to be analyzed separately.

Turning to digital effects, typically the noise power introduced by Nyquist digitization of an RF signal is given by

$$N_D = N_q + N_j \tag{2}$$

$$= \frac{V_{p-p}^2}{6RL_q^2} + P(2\pi f_c \sigma_j)^2 \tag{3}$$

where N_q is the noise power in Watts caused by quantisation of the signal, N_j is the noise power in Watts caused by jitter in the ADC, V_{p-p} is the peak-to-peak voltage of the sampled signal, R is the receiver impedance, $L_q = 2^b$ is the number of levels available to the b-bit ADC, P is the average signal power in Watts, f_c is the signal carrier frequency and σ_j is the standard deviation of the jitter time in the ADC [29]. Assuming both the quantisation and jitter noise powers are independent and distribute equally in frequency across the sampling bandwidth of the ADC, the power within a given signal bandwidth can be calculated as

$$P_{N_D} = \frac{B N_D}{f_{s_{Nyq}}} \tag{4}$$

where B is the signal bandwidth and $f_{s_{Nyq}}$ is the Nyquist sampling frequency, so the term $\frac{N_d}{f_{s_{Nyq}}}$ gives the noise power spectral density (PSD). Note the calculation of quantisation noise assumes that the signal of interest completely occupies the dynamic range of the ADC. This is often a good assumption, as only a single signal is being digitized and some form of automatic gain control (AGC) is used to ensure the peak-to-peak voltage swing of the signal is nearly equal to the ADC dynamic range. It should be noted that due to the high peak-to-average-power ratio (PAPR) of modern waveforms, in practice the signal is often clipped by the ADC at some voltage $\pm V_{clip}$ which allows some factor C, often 99%, of the waveform through [31].

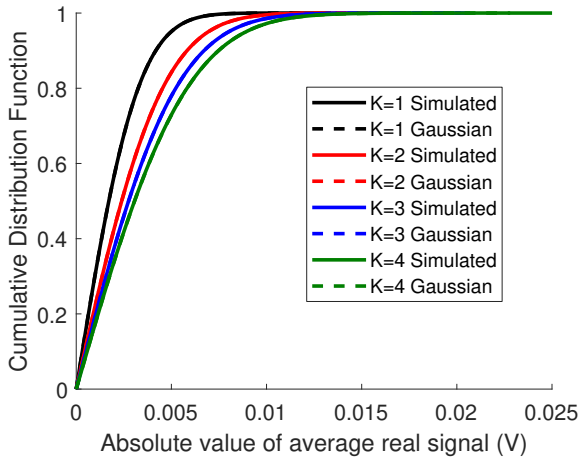

Fig. 2. Simulated CDF of K upconverted and summed LTE signals compared with Gaussian CDF with equivalent variance

However, the assumption does not hold when the sampled signal consists of multiple different signals of interest, each at a different carrier frequency and with a different power, which is the unique case treated in this paper. Here, a signal with greater power may occupy a significantly larger portion of the ADC dynamic range than the others. This can be accounted for by replacing V_{p-p} in (2) with $2V_{clip}$ where $\pm V_{clip}$ is chosen to allow factor C of the total voltage waveform $v(t)$ at the ADC input. Due to the complexity of modern waveforms, it can be assumed that $v(t)$ takes a Gaussian distribution.

This is demonstrated by modelling the 20 MHz downlink LTE signal using MATLAB's LTE toolbox when transmitting through a frequency selective multipath fading channel. For each of the K bands, 1000 LTE subframes with random data, 16-QAM modulated on to the physical downlink shared channel (PDSCH), were generated, up converted to a 50 MHz RF carrier frequency and transmitted through a frequency selective fading channel. The coherence bandwidth of the dispersive channel was matched to the LTE subcarrier bandwidth of 15.2 kHz giving independent fading per subchannel. In addition, a random signal gain between 20 dB and 30 dB, accounting for the different gains of the antenna and RF front-end in each band, is applied to each RF signal. Using a 50 MHz carrier frequency reduced the processing time without affecting the overall statistics, as the distribution of $v(t)$ is independent of carrier frequency. The K bands were circularly shifted randomly with respect to each other to mimic asynchronous downlink transmission, and summed to form the composite

TABLE I
KEY VALUES FROM STANDARD NORMAL DISTRIBUTION TABLE

C	$Pr(0 < x < z)$	z
0.90	0.45	1.645
0.95	0.475	1.960
0.99	0.495	2.575

multiband signal. The above procedure was repeated 100 times to form an ensemble of multipath impaired composite received signals for determining the cumulative distribution function (CDF) of $|v(t)|$, $Pr(|v(t)| < x)$. The CDF of $|v(t)|$ is shown in Fig. 2 for different values of K, compared with the CDF of the absolute value of zero-mean Gaussian distributions (half-normal distributions) with the same variance σ_{tot}^2 as $v(t)$. The results demonstrate that the distribution of $v(t)$ closely adheres to a Gaussian distribution.

The investigation of the distribution of $v(t)$ does not include the effect of receiver nonlinearity, for example, due to saturation of the first LNA. Under LNA compression, the received composite signal is unlikely to exhibit a Gaussian distribution. Nonlinearity would distort the signal as well as alter the parameters for predicting the digital noise effect, with the former impacting performance more. The paper assumes that $v(t)$ remains within the receivers linear region as the typical operating scenario and nonlinear effects will be treated in the authors' future work.

Therefore, $v(t)$ is treated as a Gaussian random variable with variance

$$\sigma_{tot}^2 = \sum_{k=1}^{K} \sigma_k^2 \tag{5}$$

where σ_k is the variance of the voltage signal in the kth band at the ADC input. This can be written in terms of the received power of each band at the receiver input, P_k, giving

$$\sigma_{tot}^2 = R \sum_{k=1}^{K} G_k P_k \tag{6}$$

where R is the ADC input resistance, usually 50 Ω, G_k is the receiver gain at the carrier frequency of band k, and P_k is the signal power in band k at the receiver input. From this, the clipping voltage can be determined through use of the standard normal distribution table, key values of which are shown in Table I. For a desired C and distribution $x \sim \mathcal{N}(0,1)$, the value $x = z$ to give C can be read from the table to obtain

$$V_{clip} = z\sigma_{tot} \tag{7}$$

$$= z\sqrt{R \sum_{k=1}^{K} G_k P_k} \tag{8}$$

giving an overall quantisation noise in the band of interest $k = n$ of bandwidth B_n expressed as

$$P_{q_n} = \frac{2z^2 B_n}{3L_q^2 f_{s_{Nyq}}} \sum_{k=1}^{K} P_k G_k. \tag{9}$$

Similarly for jitter noise, the assumption in (2) is that the sampled waveform is, or can be treated as, a single waveform. Assuming that the jitter noise introduced sums linearly with each carrier,

$$P_{j_n} = \frac{B_n}{f_{s_{Nyq}}} \sum_{k=1}^{K} P_k G_k (2\pi f_k \sigma_j)^2 \tag{10}$$

where f_k is the carrier frequency of band k. Note that, due to the digital noise processes being assumed as white, the digital noise is constant across all bands.

Together with RF noise, this gives the full equation for the noise within band n at the output of a Nyquist sampling ADC as

$$\begin{aligned} P_{N_n} &= \frac{B_n}{f_{s_{Nyq}}} \left(\frac{2z^2}{3L_q^2} \sum_{k=1}^{K} P_k G_k + \sum_{k=1}^{K} P_k G_k (2\pi f_k \sigma_j)^2 \right) \\ &\quad + k_B T B_n G_n F_n \\ &= \frac{B_n}{f_{s_{Nyq}}} \sum_{k=1}^{K} P_k G_k \left(\frac{2z^2}{3L_q^2} + (2\pi f_k \sigma_j)^2 \right) \\ &\quad + k_B T B_n G_n F_n \end{aligned} \tag{11}$$

This can be used to calculate the signal to noise ratio (SNR) per band, and so EVM with the relationship [32]

$$\text{EVM} \approx \frac{1}{\sqrt{\text{SNR}}}. \tag{12}$$

B. Subband Sampling

Where the ADC performs subband sampling, the conventional in-band RF noise is not the only value to be considered. Out-of-band noise becomes aliased into the in-band region, increasing the noise power present. In singleband directly digitizing receivers, we can assume that due to effective filtering of the RF signal, usually of 50dB or more, the contribution of this out-of-band aliased noise is negligible. However, in multiband receivers the filtering available often has less rejection and broader bandwidths. For the subband case, the total RF noise in band n at the output of an ideal ADC is given by

$$\begin{aligned} N_{RF_{sub_n}} = k_B T B_n \Big(& G_n F_n + (m-1) \frac{G_n}{L_{R_n}} F_{LNA_1} + \\ & + (m-1) G_{LNA_2} (F_{LNA_2} - 1) \Big) \end{aligned} \tag{13}$$

where L_{R_n} denotes the SAW filter rejection ratio corresponding to band n and $m \triangleq \left\lfloor \frac{2f_H}{f_{s_{sub}}} \right\rfloor$ is the number of times the wideband noise is folded into band B_n given $f_{s_{sub}}$ is the subsampling frequency and f_H is the highest frequency of interest, which is usually the RF bandwidth of the ADC. In (13), the first, second and third terms denote in-band noise components associated with the conventional RF noise, the folded out-of-band noise attributed to LNA_1, and the folded out-of-band noise attributed to LNA_2, respectively. The dependencies of $N_{RF_{sub_n}}$ on the RF front-end architecture and its associated parameters is discussed in more detail in Section IV-A.

In practice, the RF filtering bandwidth for each band is often wider than the signal bandwidth. This means that, even when

the sample rate and carrier frequencies have been chosen to avoid aliased signals overlapping with each other, the filter bandwidths may overlap when aliased, leading to frequency dependent noise powers at a greater value than suggested by (13). As the analysis for this process is highly contingent on the frequency domain characteristics of the RF front-end, as well as the sample rates, for clarity of analysis this process is left for future work. The effect is captured in the full numerical modelling and experimental implementation of the receiver later in this paper.

Digital noise introduced by a subsampling ADC is calculated in a similar way to the Nyquist case, giving a final subsampling noise power

$$P_{N_n} = \frac{B_n}{f_{s_{sub}}} \sum_{k=1}^{K} P_k G_k \left(\frac{2z^2}{3L_q^2} + (2\pi f_k \sigma_j)^2 \right) + N_{RF_{sub_n}}. \tag{14}$$

Comparing with (11), the term in $N_{RF_{sub_n}}$ captures the degradation in performance due to folded RF noise in the subband sampling case. As seen from (13), performance is strongly influenced by filtering quality and m. Since the RF bandwidth is fixed, a lower subsampling rate $f_{s_{sub}}$ leads to higher in-band RF noise due to more folding.

More subtle is the difference in the first term, where the digital noise is spread over the sampling bandwidth $f_{s_{sub}}$. This may be significantly lower than a Nyquist sampling rate $f_{s_{Nyq}}$, meaning the sensitivity of the subband sampling receiver would be degraded more by the presence of other bands. This effect increases as $f_{s_{sub}}$ decreases. As such, the subband multiband receiver must have a greater emphasis placed on the quality of ADC, namely the resolution and *rms* jitter, to ensure the digital noise is minimised when it is the dominant noise effect. This means there is a design choice to be made, as decreasing the sampling frequency reduces the processing required in the digital back-end of the receiver, so reducing size, weight and power consumption; but doing so increases the digital and RF noise in each band.

IV. Design of a Quadband Single-RF Chain Receiver

To demonstrate the performance of concurrent multiband radios, a receiver capable of simultaneously processing four distinct signals in four distinct bands was developed. This is an advance on the state-of-the-art triband receiver previously developed [18]. The choice of components and how they are modeled mathematically and in Simulink, using the latter to verify the analysis in Section III, are discussed in this section. The transceiver testbed provides an experimental framework for identifying the key principles for designing concurrent, multiband, direct RF sampling radio receivers.

The four carrier frequencies, f_k for $k = 1 - 4$, which the receiver is designed around, are shown in Table II. These are all allocated mobile bands in the UK: the 888 MHz band is a 3G band, 1920 MHz and 2520 MHz are LTE bands, and 3450 MHz is a 5G New Radio (NR) band. Despite the signals in these bands using different standards and having different bandwidths, for consistency of analysis the signals

TABLE II

f_k (MHz)	3GPP Band	f_{i_k} at 250 MSample/s (MHz)
888	B8	112
1920	B3	80
2520	B7	20
3450	n78	50

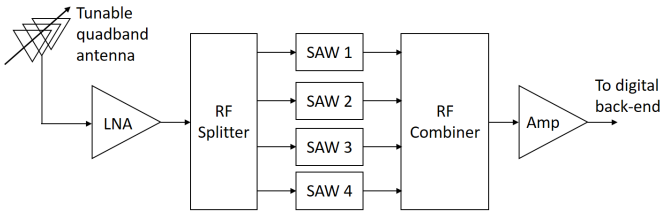

Fig. 3. Design of RF front-end for concurrent multiband receiver

TABLE III
Gains and Noise Figures for Designed RF front-end

Band k	LNA Gain (dB) [33]	LNA NF (dB)	Splitter Loss (dB) [34]	SAW Loss (dB)	G_k (dB)	NF_k (dB)
1	21.4	1.33	6.4	1.37 [35]	28.6	1.5
2	21.2	1.44	6.7	1.61 [36]	27.4	1.7
3	20.9	1.50	6.8	1.27 [37]	26.9	1.8
4	20.6	1.48	7.1	3.56 [38]	23.4	2.1

in each band will be 20 MHz LTE downlink signals with 16QAM modulation and 1/3 rate coding. In Simulink these are produced using MATLAB's LTE Toolbox, while in the mathematical analysis we let $B_k = 20$ MHz for all k.

The exact carrier frequencies are also chosen to ensure that, when subsampled, the signals do not overlap in frequency. While the details of the choice of ADC sampling rate will be discussed later in this section, the minimum used was 250 MSample/s. Note that this is constrained by the testbed hardware used, rather than being the theoretical minimum for $K = 4$ 20MHz bands. Instead, at 250 MSample/s, each signal is folded down multiple times to some intermediate frequency f_{i_k}, also shown in Table II. This gives spacing between each band of at least 10 MHz for $K = 4$ bands.

A. RF Front-End

The design of the testbed receiver RF front-end is shown in Fig. 3, and each component's gain and NF are shown in Table III, and NF_k denotes the overall NF in band k. The first component is a tunable quadband antenna previously developed by this group [39]. It consists of four resonant slots, each embedded with a varactor diode for tunability, all fed by a single port. Biasing each diode individually gives a narrowband response at each carrier frequency, providing improved rejection of unwanted signals in comparison with a wideband antenna. From the lowest band to the highest, the bias voltages are 10.0 V, 9.25 V, 14.0 V and 7.20 V, respectively. For the purposes of analysis and simulation the

TABLE IV
SAW FILTER TYPICAL PARAMETERS

Band k	Part no.	Centre freq (MHz)	Bandwidth (MHz)	Passband ripple (dB)	Rejection ratio (dB)
1	TA1889A	888.8	18	0.8	39
2	TA2018A	1900	40	0.5	29
3	TA1683A	2530	20	0.3	32
4	TA2307A	3500	200	0.4	23

antenna is omitted, as the receiver is not being evaluated in the presence of out-of-band signals so the antenna will not notably impact performance.

The following stage of the RF front-end is a first stage of amplification. Equation (14) suggests that an ideal receiver would have high gain and low NF for all four in-band signals, but low gain or high rejection outside these bands. This points to the use of a concurrent, multiband, low noise amplifier (LNA), but such devices are yet to become widely available [40], [41]. In the testbed, a Mini-circuits ZX60-83LN12+ wideband LNA is used. This amplifies all the in-band signals leaving the mitigation of the out-of-band interference and noise to a bank of $K = 4$ filters as depicted in Fig. 3.

Filtering is required to give strong out-of-band rejection to limit unwanted signals and improve noise performance. To achieve a suitable level of rejection, TAI-SAW surface acoustic wave (SAW) filters are used (Table IV). All of these have out-of-band rejection of at least 40dB. In the testbed, the concurrent multiband filtering using a bank of $K = 4$ singleband filters is realised by first splitting the RF signal using a Minicircuits ZN4PD1-63HP-S+ one-to-four splitter/combiner, then filtering each band with a SAW filter, and then recombining the signals in an identical combiner.

The filter bank configuration ensures a high level of rejection of unwanted signals. However, the RF losses due to the splitter and combiner necessitated a second stage of amplification after the combiner. To keep the experimental utility of the testbed broad, a further ZX60-83LN12+ LNA was used. The equal gains before and after filtering, resulted in a highly stable RF front-end. Also, the configuration enabled calculation of the in-band gain and NF using conventional methods [29] (Table III).

Section III-B introduced the in-band RF noise analysis for the subband sampling case. When deriving (13), the combined rejection ratios of the SAW filters (Table IV) and the multiband antenna (measured at $\geq$ 3dB) is considered sufficient to remove out-of-band RF noise and interference. As the thermal noise generated by LNA_1 is also SAW filtered, providing each filter's out-of-band rejection ratio L_{R_n} exceeds the subsampling folding factor $(m-1)$, the contribution of LNA_1's out-of-band noise is small. In the testbed, the same LNA type was used for the first and second stage amplifiers. For this configuration, the worse case out-of-band performance of a SAW filter corresponds to band 4 at 3450 MHz (Table III). Applying (13) to band 4 with $m = 40$ gives $G_4F_4 = 25,53$dB, $(m-1)\frac{G_4}{L_{R_4}}F_{LNA_1} = 17.83$dB and $(m-1)G_{LNA_2}(F_{LNA_2}-1) = 32.6$dB. That is, for the front-end architecture considered, the dominant noise effect with subsampling is due to the spectral folding of LNA_2's out-of-band noise. Options to keep this noise level low include minimising F_{LNA_2}, splitter/combiner losses and SAW filter insertion losses; designing $G_{LNA_1} > G_{LNA_2}$; and restricting the folding factor $(m-1)$. All of these options involve a trade-off between system and component performance.

In the analysis, the noise figure of the ADC was neglected since the noise is dominated by the RF front-end. Together with Table III this is all the required information for mathematical modelling of the realised RF front-end of the concurrent multiband receiver.

B. Digital Back-End

The ADC should have an RF bandwidth covering the range of bands required, and it should be able to achieve the desired sample rate. For flexibility in the testbed, a LeCroy WaveMaster 813Zi-A oscilloscope was used. Its resolution is 8 bits, and it has a maximum RF bandwidth of 13 GHz. For the purposes of this investigation, the 4 GHz input filter option was always used, which comfortably allows the highest 3.45 GHz band to be accurately reconstructed. In the mathematical modelling, this means that $f_H = 4$ GHz. Note that this bandwidth is available only for peak-to-peak voltage ranges greater than 0.08 V, decreasing at low signal powers.

The oscilloscope's maximum sample rate is 40 GSample/s, with flexibility to reduce this programmatically to $1\times$, $2.5\times$ and $5\times$ each power of 10 Sample/s. As such, 10 GSample/s was chosen for Nyquist sampling, as it is the lowest available rate at which Nyquist sampling is obtained for all bands, although the theoretical lower limit is 6.92 GSample/s due to the 3.45 GHz band and 20 MHz LTE signal. Similarly, for subband sampling, 250 MSample/s was chosen, though the theoretical lower limit for receiving four 20 MHz signals concurrently with 1 MHz guard bands is 168 MSample/s.

A reconfigurable subband receiver may need to process different combinations of carrier frequencies and, therefore, adapt its common subsampling rate to avoid the spectral overlap of concurrent multiband signals. Presently, there is still no closed form solution for selecting such a common subsampling rate [22]. Solutions are usually found numerically, for example, in mobile networks edge computing at the base station could run an exhaustive search algorithm and communicate the sampling parameters via higher layer control signaling when radio bearers are set up or changed. As such, subband sampling for software defined radios is an active research area.

The sampled signals are each downconverted using DDCs consisting of digital numerically controlled oscillators (NCOs) followed by low-pass filters to extract the desired baseband signal. In the Nyquist case, the NCOs are centred at f_k while in subband sampling they are centred at f_{i_k}, for $k = 1, 2 \ldots 4$. Note that for mathematical modelling ideal brick-wall filtering is assumed around the 20 MHz bandwidth of the signal, whereas in the experimental testbed implementation using an NI PXIe-8135 chassis - used to allow real-time FPGA operation - finite impulse response filters are used. At 10 GSample/s the filters consist of 728 taps, whereas at 250 MSample/s 183 taps are used.

Finally, the baseband signals are processed using LabVIEW's LTE Application Framework (LTE-AF). The physical downlink shared channel (PDSCH) is extracted and the constellation's EVM is measured. Also, the transport channel is decoded and an average BLER is calculated for each channel.

C. Implementation Considerations

The receiver architecture in this paper was implemented using commercial off the shelf (COTS) components to provide a stable HWIL RF testbed for investigating the performance of concurrent multiband direct RF sampling receivers. The design prioritised minimising RF component count while mitigating out-of-band noise effects over RF blocker resilience, the later being aided by the rejection capability of the tunable muliband slot antenna used. Recent developments in both concurrent multiband filters (MBFLTs) [42] and concurrent multiband LNAs (MBLNAs) [41] could support alternative architectures with fewer RF components and greater reconfigurability. The analysis in this paper provides a new framework for investigating the efficacy of these emerging techniques.

Replacing the SAW filter bank with an integrated concurrent MBFLT in the proposed design would remove the requirement for individual splitters and combiners thereby avoiding the losses due to these components. Also, providing the MBFLT in-band insertion losses are small, the second LNA could be discarded while still supporting both Nyquist and subband direct RF sampling. To enhance the receiver's blocker resilience, the MBFLT could be placed before a single wideband LNA. This configuration would support Nyquist sampling but a high sampling rate would be required with subband sampling to limit the number of times the out-of-band LNA noise is folded.

A receiver architecture based on an MBFLT followed by an MBLNA provides both blocker resilience and alleviation of the out-of-band LNA noise. Also, the MBLNA mitigates the requirement for stringent MBFLT rejection ratios. For good blocker resilience, the MBFLTs bandwidths should match the bandwidths of the allocated bands while for good subband performance the MBLNA bandwidths should match the bandwidths of the allocated channels. In these architectures, tunable MBFLTs and MBLNAs would enable greater frequency flexibility of the receiver.

Currently, suitable concurrent MBFLTs and concurrent MBLNAs are not available as COTS components whereas researched MBFLTs and MBLNAs exhibit several limitations. For example, the number of concurrent bands available, their selectivity and tunability range, and the ability to reconfigure bandwidth are restricted. Given the large variety of architectures and types of MBFLTs and MBLNAs, a detailed evaluation of receiver performance achievable is left to future investigation.

V. Modeled Performance

In order to validate the mathematical analysis in Section III, a model was constructed in Simulink of the designed receiver (Fig. 4). For test purposes, four independent LTE baseband signals are generated using MATLAB's LTE Toolbox. Note that for ease of simulation these are synchronised, though

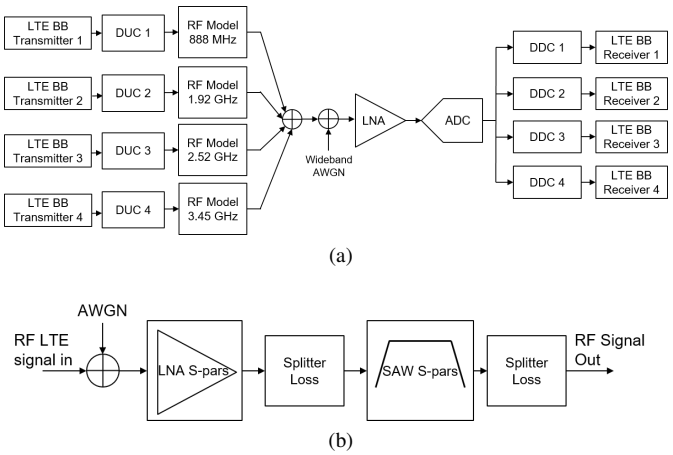

Fig. 4. Simulation model for evaluating receiver performance, (a) Model overview, (b) RF model

they do not need to be for operation. They are then digitally upconverted (DUC k in Fig. 4a) to the four carrier frequencies of interest.

Each upconverted signal is presented to a Simulink RF Blockset model (Fig. 4b). The branches are simulated separately, each centred at f_k, rather than as a single 10 GSample/s model, in order to reduce simulation time. They are each simulated over 1 GHz as this is the defined bandwidth of the SAW filter S-parameters used. Each RF model consists of additive white Gaussian noise (AWGN), S-parameter models of the first LNA and appropriate SAW filter, and ideal attenuation blocks representing the loss through the RF splitters as defined in Table III. The AWGN is assumed to be thermal noise at a temperature T =270K.

The output of each of these narrowband models is then summed, and wideband AWGN at T =270K is added before applying an S-parameter model of the second LNA. This ensures the spectrum between the narrowband models contains the appropriate level of noise while having minimal effect on the noise power within the SAW filter bands.

This wideband waveform is passed to an ADC, which is modeled as a first-order low-pass filter with 4 GHz bandwidth, equivalent to the bandwidth of the oscilloscope; followed by a voltage limiter defining the peak-to-peak voltage of the input signal, a sampler at 10 GSample/s, a downsampler for use in the subband sampling case, and finally an 8-bit quantiser, equivalent to the resolution of the oscilloscope. Note that this introduces quantisation noise but not jitter noise. The quantised signal is presented to the four DDCs for digital downconversion and lowpass filtering. The four resultant baseband waveforms are processed to retrieve the PDSCH constellation's EVM and the transport channel BLER using the LTE Toolbox.

To evaluate the performance of the testbed receiver, two key scenarios will be investigated: singleband and multiband operation. In both cases, the SNR will be calculated for each possible band of interest as discussed in Section III, and an estimate of the EVM obtained using (12). The calculated SNR will then be used in a MATLAB baseband LTE downlink simulation to obtain a BLER [43]. In the paper, these results

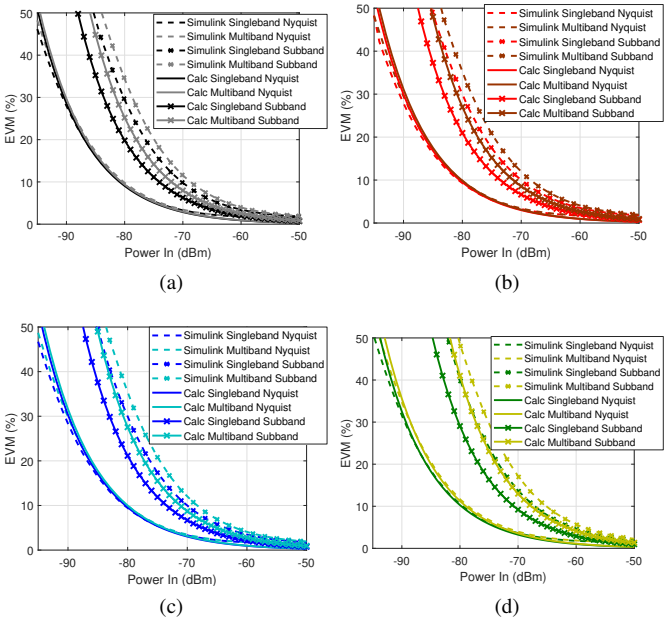

Fig. 5. EVM performance of multiband receiver comparing mathematical model (Calc) and Simulink RF model (Simulink) for Nyquist (10 GSample/s) and subband (250 MSample/s) sampling, and singleband and concurrent multiband operation. (a) 888 MHz band, (b) 1920 MHz band, (c) 2520 MHz band, (d) 3450 MHz band.

are referred to as baseband modeled BLER. This will be compared with the EVM and BLER results from the Simulink model, which incorporates the RF front-end, for the same cases. These results are referred to as simulated EVM and BLER. Results will be obtained with Nyquist sampling (10 GSample/s), and subband sampling (250 MSample/s). In the singleband case, the received power in the band of interest is varied while the received power in the other bands is set to zero.

To evaluate the receiver in concurrent multiband operation, an adapted version of the adjacent channel selectivity test in the LTE 3GPP standard is used [44]. This test states that where a signal is in the presence of an adjacent channel with 39dB greater power than the reference sensitivity level of the desired signal, the 95% throughput point of the desired signal should degrade by less than 14dB. The scenario under test in this paper is different, as for each signal of interest there are three interfering signals, which are still required for multiband operation, not immediately adjacent to the signal of interest. Nonetheless, the test meets the criterion of the receiver not being explicitly designed to filter out the interferes, and so is a rigorous benchmark for evaluation of concurrent multiband performance in a single radio receiver.

In the concurrent multiband measurement, three bands will be set to a high receive power while the receive power of a single band of interest is varied to find the degradation caused by the presence of the other signals. In previous measurements the reference sensitivity point for the 888 MHz band was found to be -89dBm [44], so for consistency all bands not of interest will be set to -50dBm received power. This is done for both 10 GSample/s and 250 MSample/s cases.

The calculated and simulated EVMs are shown for all cases and all bands in Fig. 5. In all four bands, the singleband Nyquist case shows very good agreement between the mathematical and Simulink model, helping validate the analysis. The simulated EVMs decrease to 1.6% for both singleband and multiband operation while calculated EVMs decrease to around 0.3% in both cases, suggesting a floor on component modelling. The EVMs reach the 12.5% required for 16-QAM operation in LTE at approximately -83dBm for the 888 MHz band, -82dBm for the 1.92 GHz and 2.52 GHz bands, and -81dBm for the 3.45 GHz band [44]. In the multiband Nyquist case there is still close agreement, with small deviation from the singleband case for the lowest three bands. This suggests that the additional quantisation noise (and in the mathematical calculations, jitter noise) introduced by the desensitized ADC is spread out over the 5 GHz Nyquist bandwidth, ensuring it remains below the in-band RF noise. There is slight degradation of approximately 1dB in the 3.45 GHz band, most likely as the higher gain of the other three bands tabulated in Table III introduces greater desensitization at the ADC, while the in-band noise floor is slightly lower, resulting in quantisation noise impacting more in this band.

There is some loss in agreement between calculation and simulation in the subband sampling cases. For a target EVM of 12.5%, the degradation of singleband subband operation compared with singleband Nyquist operation is calculated as approximately 6dB in the lower three bands and 9dB in the 3.45 GHz band, while the simulated degradation is a further 4dB for the lower three bands and around 3dB for the 3.45 GHz band. This is mostly due to the effect of overlapping SAW filter bandwidths, as introduced in Section III. The simulation models the effect of greater RF noise caused by the SAW filter bandwidths aliasing onto the wanted signal bandwidth, while this is not accounted for in the calculation. Using the S-parameters of the specific SAW filters used here, and $f_s = 250$ MSample/s, the contribution to the noise of these filters can be calculated separately. This gave an increase in noise of 2.4dB, 2.1dB, 1.8dB and 2.0dB for bands $k = 1$ to 4, respectively, which maps closely onto the observed differences in performance. Even more accurate results may be obtained by including the varying gain and noise figure of the LNA across the whole operating range. Closer matching of the SAW filter bandwidths to the signal bandwidths would reduce the SNR degradation caused by this effect.

The degradation from singleband subband operation to multiband subband is consistent between the calculated and simulated EVMs, further validating the analysis. This is approximately 2dB for $k = 1$ with both simulated and calculated, but for $k = 2$ to 4 the calculated degradation is approaching 3dB whereas the simulated degradation is approximately 2dB. This is consistent with the RF noise being slightly higher in the simulated case, and so obscuring some of the degradation expected by the calculated increase in quantisation noise due to ADC desensitization.

These baseband modeled BLERs are compared with the simulated BLER curves in Fig. 6, and show similar trends to the EVM performance. Again the singleband Nyquist and multiband Nyquist BLER performances are closely matched between baseband and Simulink models, with most being

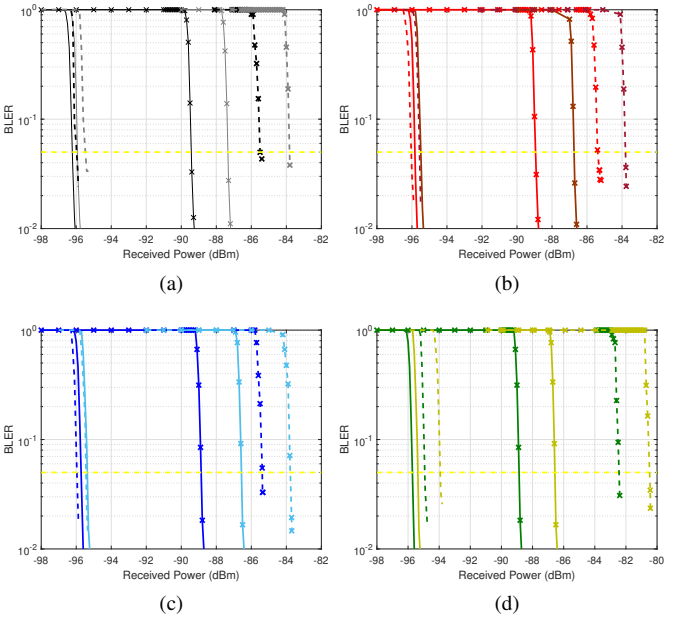

Fig. 6. BLER performance of multiband receiver comparing baseband model and Simulink RF model for Nyquist (10 GSample/s) and subband (250 MSample/s) sampling, and singleband and concurrent multiband operation. See Fig. 5 for legend. (a) 888 MHz band, (b) 1920 MHz band, (c) 2520 MHz band, (d) 3450 MHz band.

within 0.2dB and the largest discrepancy being at 3.45 GHz with 1.4dB variation. The key trends are also the same, with around 9dB degradation in the baseband case from singleband Nyquist to multiband subband for all frequencies, increasing to around 13dB when the Simulink model includes the effect of overlapping SAW filter bandwidths. This helps validate both models for understanding the noise processes in concurrent multiband direct sampling receivers.

VI. Hardware-in-the-Loop Implementation

A. Cable Connection Testbed

The receiver was then implemented in a HWIL testbed (Fig. 7). Three bands were transmitted independently from an NI PXIe 8135 controller, outputting 20 MHz downlink LTE signals with 16QAM modulation on their physical channels, and 1/3 rate coding. One band is transmitted using an NI-5793 FlexRIO RF Adapter Module controlled by LabVIEW's LTE Application Framework (LTE-AF), and two using two NI-5791 FlexRIO RF Adapter Modules controlled by separate LabVIEW transmitters. The final band is provided by a Rohde & Schwarz SMBV100a signal generator, and produces 20 MHz 802.11g signals with 16QAM modulation on each subcarrier. This underlines the multistandard nature of this receiver design. Note that the transmit power, modulation and input data for each of these signals is completely independent, and none of these four signals was synchronized with the others, thereby emulating a downlink, quad-connectivity, heterogeneous network use case. The signals were combined using three Mini-circuit ZAPD-2-272-S+ 2-signal combiners, and connected by coaxial cable straight into the first LNA of the receiver's RF front-end. This was done to focus on

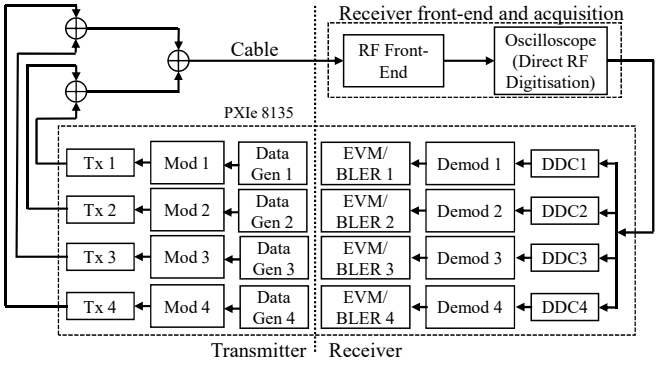

Fig. 7. HWIL testbed for evaluation of concurrent multiband receiver using cabled connections

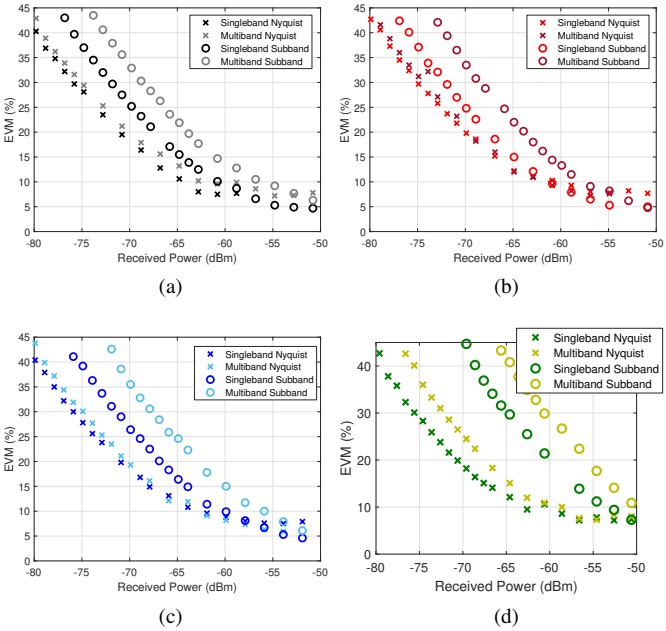

Fig. 8. Measured EVM against received power with Nyquist and subband sampling, for singleband and multiband cases, for bands (a) 888 MHz, (b) 1920 MHz, (c) 2520 MHz, (d) 3450 MHz

the noise processes in the receiver by minimising nonlinear impairments introduced by transmitter amplification. Also, the impact of the multiband antenna on system performance does not need to be taken into account in the analysis.

The signals then pass through the RF front-end discussed in Section IV-A for amplification and filtering, and sampled by the LeCroy WaveMaster oscilloscope at either 10 GSample/s (Nyquist) or 250 MSample/s (Subband) in 10 ms frames. Digital downconversion and channel filtering occurs in the NI PXI, before only the signal from the LabVIEW LTE-AF is processed using LabVIEW to retrieve the PDSCH constellation producing an EVM measurement, and decode the transport layer to obtain a BLER. The power of the LTE-AF transmitter is varied, while the other transmitters are either switched off (singleband operation) or transmitting so the received power in each band at the input to the RF front-end is -50dBm (multiband operation).

The measured EVMs are shown in Fig. 8. When compared

with the modeled EVMs in Fig. 5, there is a higher received power needed for an equivalent EVM. This can be explained by the noise output of the transmitters being -130dBm/Hz, significantly above the -174dBm/Hz noise power spectral density assumed for the whole receiver in the modelling at 270K. This can be accounted for in the mathematical and Simulink models by having a higher noise temperature at the input to the first LNA than at the second LNA. Also note that the measured EVM seems to fall quicker with increasing signal power at first. This is due to EVM measurements in the testbed only being taken when synchronisation is successful, which at low SNRs favours better EVMs than expected being measured. Finally, the EVM floor in the testbed is higher than in the modelling, at around 5%, and is found not to reduce even with signal powers above -50dBm. This is due to a combination of a range of sources, such as synchronization inaccuracies in the ADC, which when propagated through digital downconversion, filtering and OFDM demodulation may lead to significant random noise. Other sources include jitter and the analogue front-end of the oscilloscope. Nonetheless, the EVM floor remains substantially below the 12.5% required for reliable 16QAM operation.

Importantly, the key trends follow a very similar pattern to the modeled results in Section V, with the singleband Nyquist reaching 12.5% EVM at the lowest power. Adding in other high-powered bands degrades the performance negligibly for the 888 MHz and 1920 MHz bands, by 1dB for the 2520 MHz band and 2dB for the 3450 MHz band. This compares favourably with the mathematical and Simulink models which predicted between 0.5dB and 1dB degradation, again increasing with the band frequency. The singleband subband case requires 4dB more power than Nyquist for the bottom three bands, which increases to 10dB at the top band, which is largely due to the folded RF noise and SAW filter bandwidths. These then degrade between 3dB and 4dB in all bands when moving to multiband subband operation, which is similar to the 2 to 3dB difference predicted by both modelling techniques. This further validates the mathematical model for use in multiband receiver design processes.

Similarly, BLER measurements are shown in Fig. 9. Note that the BLER begins to fall at around 40% EVM in the testbed, while in the modeled results in Fig. 6 they begin to fall at around 60% EVM. Further, compared with modeled results the measured BLER takes a greater increase in power to fall below 5%. This is due to the extra synchronization required in the testbed leading to higher SNRs being required to successfully decode the waveform. The maximum degradation between singleband and multiband for 95% throughput is 2dB for Nyquist sampling and 3dB for subband sampling, both well within the LTE standard for concurrent reception. As such both receivers could be considered for practical use, with the potential to enhance receiver sensitivity by closer matching the signal and SAW channel filter bandwidths for a given subsampling rate.

In order to evaluate how the performance of the subband sampling receiver alters with different sampling rates, the EVM was measured for the 888 MHz and 3450 MHz bands while the other signals are received at -50dBm (Fig. 10).

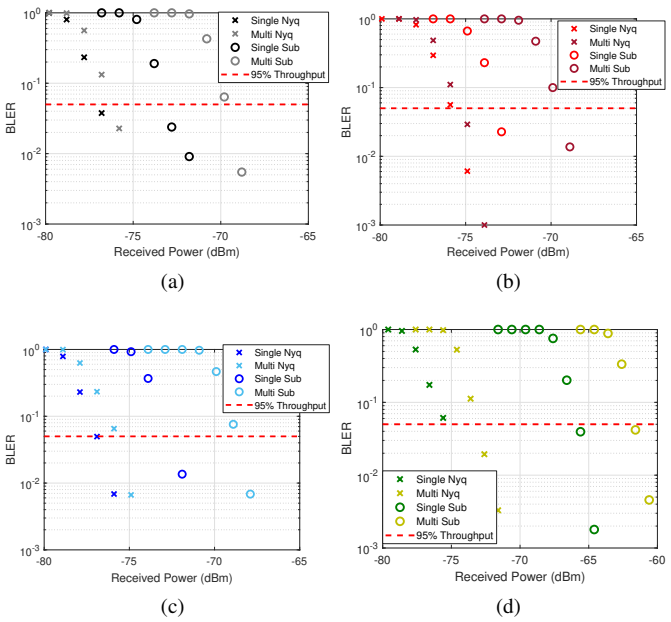

Fig. 9. Measured BLER against received power with Nyquist and subband sampling, for singleband and multiband cases, for bands (a) 888 MHz, (b) 1920 MHz, (c) 2520 MHz, (d) 3450 MHz

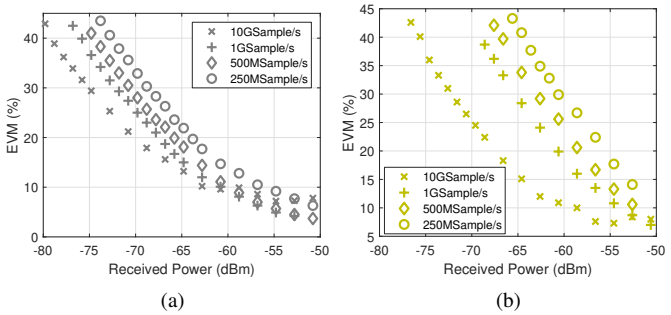

Fig. 10. Measured EVM against received power in multiband case for different sampling rates, for bands (a) 888 MHz, (b) 3450 MHz

Nyquist sampling at 10 GSample/s is included for reference. As expected decreasing the sampling rate increases the degradation in performance due to increased RF noise folding, increased in-band digital noise and increased noise spectra overlap associated with the SAW channel filters. The effect is more noticeable in the 3450 MHz band, which has a higher noise figure, lower gain in its RF front-end and much wider SAW channel filter bandwidth.

B. Over-the-Air Testbed

Finally, the HWIL testbed receiver was evaluated in an over-the-air (OTA) measurement configuration (Fig. 11). This is identical to the cable measurements, except the combined transmitted signals are now passed through a Pasternack PE15A4019 wideband power amplifier (PA) and then through a wideband horn antenna. This antenna is positioned 2m away from the multiband antenna described in Section IV-A, which is biased at 10.0V, 9.25V, 14.0V and 7.2V for bands $k = 1$ to 4, respectively, to ensure resonance at each of the four carrier

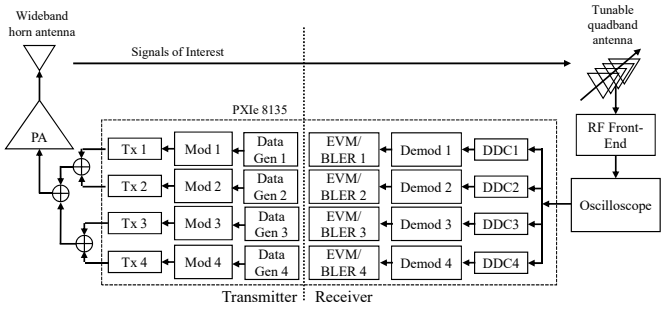

Fig. 11. OTA HWIL testbed for evaluation of concurrent multiband receiver

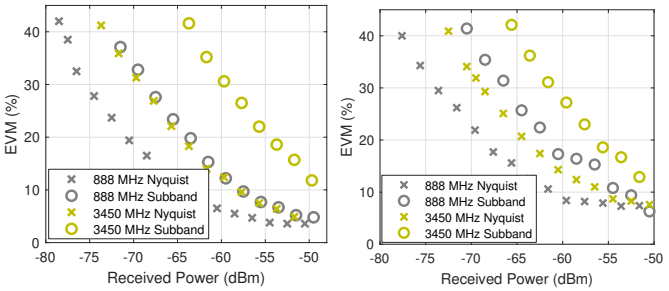

Fig. 12. Multiband EVM measurements in OTA testbed for 888 MHz and 3450 MHz bands, at 10 GSample/s Nyquist and 250 MSample/s subsampling rates, (a) in an anechoic chamber, (b) in an office environment

frequencies used in the testbed. The received signal from this antenna is passed back into the receiver's RF front-end. The experiment was undertaken in both an anechoic chamber, for repeatability of investigation, and in an office environment, to ensure the results hold for a reflective environment.

The multiband performance of both Nyquist sampling at 10 GSample/s and subband sampling at 250 MSample/s were investigated for the 888 MHz and 3450 MHz bands. The measured EVMs are shown in Fig. 12. In the anechoic chamber, with Nyquist sampling the 12.5% EVM is reached at around -66dBm for the 888 MHz band and -60dBm for the 3450 MHz band, which is 2dB lower and 3dB higher, respectively, than the same measure in the cabled testbed (Fig. 12a). This is due to the PA in the OTA testbed producing a different noise profile to that produced by the NI transmitters alone.

At 250 MSample/s, the performance degrades by approximately 5dB for the lowest band and nearly 10dB for the highest band. This is slightly improved over the 6dB and 11dB, respectively, seen in the cabled testbed. This is due to the narrowband multiband antenna, which provides at least 3dB out-of-band rejection of the wideband noise produced by the NI transmitters and the PA, whereas in the cabled testbed the majority of the noise from the NI transmitters reached the SAW filters. The effect largely occurs in the top band, as Band 4's SAW filter has a 200 MHz bandwidth whereas the antenna's bandwidth at that frequency is 25 MHz. A similar, or even greater, effect would be observed by matching the SAW filter bandwidth to the signal bandwidth more closely. The subband sampled 3450 MHz band only reaches below 12.5% at over -50dBm transmit power, but continues to decrease as the received power increases beyond this point.

In the reflective office environment, the absolute measured values differ slightly due to the gain differences between channels caused by predominantly static fading (Fig. 12b). In comparison with Fig. 12a, the Nyquist sampled 888 MHz band shows 3dB degradation at 12.5% EVM, whereas the 3450 MHz band requires almost the same received power. This suggests the 888MHz channel is experiencing some frequency selective fading. For subband sampling, the degradation is $\approx$ 9dB in both the 888MHz and 3450MHz bands. For 888 MHz, the degradation is larger than in the chamber measurements, which most likely is due to the different noise profile experienced in the reflective environment.

VII. Conclusion

Analysis, modelling and experimental implementation of a concurrent, multiband, directly digitizing receiver for wideband signals has been carried out. The theoretical bases of concurrent multiband receivers were explored, leading to a new mathematical analysis for estimating key system performance indicators under both Nyquist and subsampling conditions. This was validated with a Simulink model, which also allowed exploration of the limitations of the mathematical approach. Finally, a hardware-in-the-loop testbed was constructed, and demonstrated that multiband receivers can operate successfully under harsh concurrent reception conditions, with maximum 2dB degradation for 95% throughput from singleband to multiband operation with Nyquist sampling, and maximum 3dB degradation with 250 MSample/s subband sampling, which is easily within the 14dB requirement of the LTE standard. Future work should explore performance under adjacent channel interference from unwanted signals and utilising tunable multiband filters for improved performance.

Acknowledgment

The work reported was financially supported by the UK's "Engineering and Physical Sciences Research Council" (EPSRC) on grant numbers EP/M013723/1 and EP/S008101/1.

References

[1] 3GPP, "NR intra band Carrier Aggregation (CA) Rel-16 for xCC Down Link (DL) / yCC Up Link (UL) including contiguous and non-contiguous spectrum (x $\geq$ y)," 3GPP, Tech. Rep. 38.716-01-01, 2020, release 16.

[2] H. Okazaki, A. Fukuda, K. Kawai, T. Furuta, and S. Narahashi, "MEMS-based reconfigurable RF front-end architecture for future band-free mobile terminals," in *2007 European Conference on Wireless Technologies*, 2007, pp. 300–303.

[3] P. Bahramzy, P. Olesen, P. Madsen, J. Bojer, S. Caporal Del Barrio, A. Tatomirescu, P. Bundgaard, A. S. Morris III, and G. F. Pedersen, "A tunable RF front-end with narrowband antennas for mobile devices," *IEEE Transactions on Microwave Theory and Techniques*, vol. 63, no. 10, pp. 3300–3310, 2015.

[4] W. Saad, M. Bennis, and M. Chen, "A vision of 6G wireless systems: Applications, trends, technologies, and open research problems," *IEEE Network*, pp. 1–9, 2019.

[5] L. Sundström, M. Anderson, R. Strandberg, S. Ek, J. Svensson, F. Mu, T. Olsson, I. u. Din, L. Wilhelmsson, D. Eckerbert, and S. Mattisson, "A receiver for LTE Rel-11 and beyond supporting non-contiguous carrier aggregation," in *2013 IEEE International Solid-State Circuits Conference Digest of Technical Papers*, 2013, pp. 336–337.

[6] H. Hashemi and A. Hajimiri, "Concurrent multiband low-noise amplifiers-theory, design, and applications," *IEEE Transactions on Microwave Theory and Techniques*, vol. 50, no. 1, pp. 288–301, 2002.

[7] R. Chen and H. Hashemi, "Reconfigurable receiver with radio-frequency current-mode complex signal processing supporting carrier aggregation," *IEEE Journal of Solid-State Circuits*, vol. 50, no. 12, pp. 3032–3046, 2015.

[8] E. Arabi, C. Gamlath, K. A. Morris, and M. A. Beach, "Analysis of the coverage of tunable matching networks for the imperfect matching case," *IEEE Transactions on Circuits and Systems II: Express Briefs*, vol. 66, no. 4, pp. 572–576, 2019.

[9] H. Darabi, A. Mirzaei, and M. Mikhemar, "Highly integrated and tunable RF front ends for reconfigurable multiband transceivers: A tutorial," *IEEE Transactions on Circuits and Systems I: Regular Papers*, vol. 58, no. 9, pp. 2038–2050, 2011.

[10] A. O. Olopade, A. Hasan, and M. Helaoui, "Concurrent dual-band six-port receiver for multi-standard and software defined radio applications," *IEEE Transactions on Microwave Theory and Techniques*, vol. 61, no. 12, pp. 4252–4261, 2013.

[11] S. Lee, D. Jeong, H. Jin, and B. Kim, "Reconfigurable 4 channel carrier aggregation receiver using harmonic recombination technique," in *2016 11th European Microwave Integrated Circuits Conference (EuMIC)*, 2016, pp. 1–4.

[12] A. Kale, S. Popuri, M. Koeberle, J. Sturm, and V. S. R. Pasupureddi, "A -40 dB EVM, 77 MHz dual-band tunable gain sub-sampling receiver front end in 65-nm CMOS," *IEEE Transactions on Circuits and Systems I: Regular Papers*, vol. 66, no. 3, pp. 1166–1179, 2019.

[13] J. Mitola, "The software radio architecture," *IEEE Communications Magazine*, vol. 33, no. 5, pp. 26–38, 1995.

[14] J. R. G. Oya, A. Kwan, F. M. Ghannouchi, S. A. Bassam, and F. M. Chavero, "Design of dual-band multistandard subsampling receivers for optimal SNDR in nonlinear and interfering environments," *IEEE Transactions on Instrumentation and Measurement*, vol. 63, no. 4, pp. 981–983, 2014.

[15] R. Barrak, A. Othman, G. I. Abib, M. Muller, M. Mabrouk, and A. Ghazel, "Design of a tunable anti-aliasing filter for multistandard RF subsampling GNSS receivers," *IEEE Transactions on Circuits and Systems II: Express Briefs*, vol. 66, no. 2, pp. 207–211, 2019.

[16] *12-Bit, 6 GSPS/10.25 GSPS, JESD204B, RF Analog-to-Digital Converter*, Analog Devices, 2020, rev. A. [Online]. Available: https://www.analog.com/media/en/technical-documentation/data-sheets/AD9213.pdf

[17] R. Singh, Q. Bai, T. O'Farrell, K. L. Ford, and R. J. Langley, "Concurrent, multi-band, single-chain radio receiver for high data-rate HetNets," in *2017 IEEE 86th Vehicular Technology Conference (VTC-Fall)*, 2017, pp. 1–5.

[18] S. Henthorn, T. O'Farrell, S. Asif, M. R. Anbiyaei, and K. Ford, "Tri-band single chain radio receiver for concurrent radio," in *2020 2nd 6G Wireless Summit (6G SUMMIT)*, 2020, pp. 1–5.

[19] L. Kull, D. Luu, P. A. Francese, C. Menolfi, M. Braendli, M. Kossel, T. Morf, A. Cevrero, I. Oezkaya, H. Yueksel, and T. Toifl, "CMOS ADCs towards 100 GS/s and beyond," in *2016 IEEE Compound Semiconductor Integrated Circuit Symposium (CSICS)*, 2016, pp. 1–4.

[20] C.-H. Tseng and S.-C. Chou, "Direct downconversion of multiband RF signals using bandpass sampling," *IEEE Transactions on Wireless Communications*, vol. 5, no. 1, pp. 72–76, 2006.

[21] J. Thabet, R. Barrak, A. Ghazel, and F. M. Ghannouchi, "Generalized bandpass sampling algorithm for multiband wireless receivers suitable for SDR applications," *Circuits, Systems, and Signal Processing*, vol. 36, no. 3, pp. 1099 – 1114, 2017.

[22] Y. Lin, Y. Liu, and S. Phoong, "A new iterative algorithm for finding the minimum sampling frequency of multiband signals," *IEEE Transactions on Signal Processing*, vol. 58, no. 10, pp. 5446–5450, 2010.

[23] A. G. Dempster, "Quadrature bandpass sampling rules for single- and multiband communications and satellite navigation receivers," *IEEE Transactions on Aerospace and Electronic Systems*, vol. 47, no. 4, pp. 2308–2316, 2011.

[24] S. Bose, V. Khaitan, and A. Chaturvedi, "A low-cost algorithm to find the minimum sampling frequency for multiple bandpass signals," *IEEE Signal Processing Letters*, vol. 15, pp. 877–880, 2008.

[25] J. Bae and J. Park, "A searching algorithm for minimum bandpass sampling frequency in simultaneous down-conversion of multiple RF signals," *Journal of Communications and Networks*, vol. 10, no. 1, pp. 55–62, 2008.

[26] Y. Zhao and S. Xiao, "Sparse multiband signal acquisition receiver with co-prime sampling," *IEEE Access*, vol. 6, pp. 25 261–25 269, 2018.

[27] X. Huang, X. Zhao, and J. Ma, "Joint carrier and DoA estimation for multi-band sources based on sub-nyquist sampling coprime array with large time lags," *Signal Processing*, vol. 195, p. 108466, 2022. [Online]. Available: https://www.sciencedirect.com/science/article/pii/S0165168422000135

[28] K. S. Gilhousen, I. M. Jacobs, R. Padovani, A. J. Viterbi, L. A. Weaver, and C. E. Wheatley, "On the capacity of a cellular CDMA system," *IEEE Transactions on Vehicular Technology*, vol. 40, no. 2, pp. 303–312, 1991.

[29] Q. Gu, *RF system design of transceivers for wireless communications*. Springer Science & Business Media, 2006.

[30] K. Wong and T. O'Farrell, "Coverage of 802.11g WLANs in the presence of Bluetooth interference," in *14th IEEE Proceedings on Personal, Indoor and Mobile Radio Communications, 2003. PIMRC 2003.*, vol. 3, 2003, pp. 2027–2031 vol.3.

[31] Xiaodong Li and L. J. Cimini, "Effects of clipping and filtering on the performance of OFDM," in *1997 IEEE 47th Vehicular Technology Conference. Technology in Motion*, vol. 3, 1997, pp. 1634–1638 vol.3.

[32] R. A. Shafik, M. S. Rahman, and A. R. Islam, "On the extended relationships among EVM, BER and SNR as performance metrics," in *2006 International Conference on Electrical and Computer Engineering*, 2006, pp. 408–411.

[33] *Low Noise Amplifier ZX60-83LN12+*, Minicircuits, 2017, rev. 1. [Online]. Available: https://www.minicircuits.com/pdfs/ZX60-83LN12+.pdf

[34] *High Power, DC Pass Power Splitter/Combiner ZN4PD1-63HP-S+*, Minicircuits, 2017, rev. 1. [Online]. Available: https://www.minicircuits.com/pdfs/ZN4PD1-63HP+.pdf

[35] *Product Specifications Approval Sheet: SAW Filter 888.75 MHz*, Tai-SAW Technology Co., 2015, rev. 1. [Online]. Available: https://www.taisaw.com/upload/product/TA1889A\%20_Rev.1.0_.pdf

[36] *Product Specifications Approval Sheet: SAW Rx Filter 1900 MHz LTE Band 39*, Tai-SAW Technology Co., 2017, rev. 2. [Online]. Available: https://www.taisaw.com/upload/product/TA2018A\%20_Rev.2.0_.pdf

[37] *Product Specifications Approval Sheet: SAW Filter 2530 MHz 20 MHz Bandwidth*, Tai-SAW Technology Co., 2013, rev. 1. [Online]. Available: https://www.taisaw.com/upload/product/TA1683A\%20_Rev.1.0_.pdf

[38] *Product Specifications Approval Sheet: SAW Filter 3500 MHz*, Tai-SAW Technology Co., 2017, rev. 1. [Online]. Available: https://www.taisaw.com/upload/product/TA2307A\%20_Rev.1.0_.pdf

[39] S. M. Asif, M. R. Anbiyaei, K. L. Ford, T. O'Farrell, and R. J. Langley, "Low-profile independently- and concurrently-tunable quad-band antenna for single chain sub-6GHz 5G New Radio applications," *IEEE Access*, vol. 7, pp. 183 770–183 782, 2019.

[40] M. A. Beach, L. Laughlin, E. Arabi, S. Wilson, S. Ozan, and C. Gamlath, "Enabling RF technologies for spectrum sharing," in *2020 14th European Conference on Antennas and Propagation (EuCAP)*, 2020, pp. 1–5.

[41] A. Aneja and X. J. Li, "Multiband LNAs for software-defined radios: Recent advances in the design of multiband reconfigurable LNAs for SDRs in CMOS, microwave integrated circuits technology," *IEEE Microwave Magazine*, vol. 21, no. 7, pp. 37–53, 2020.

[42] D. J. Simpson, R. Gómez-García, and D. Psychogiou, "Tunable multi-band bandpass-to-bandstop RF filters," in *2018 IEEE/MTT-S International Microwave Symposium - IMS*, 2018, pp. 1363–1366.

[43] S. Henthorn, "Dataset and code for "concurrent multiband direct RF sampling receivers"," https://figshare.com/s/7d484066840815f14567.

[44] 3GPP, "LTE; Evolved Universal Terrestrial Radio Access (E-UTRA); User Equipment (UE) conformance specification; Radio transmission and reception; Part 1: Conformance testing (3GPP TS 36.521-1 version 12.3.0 Release 12)," 3GPP, Standard, 2014.

Stephen Henthorn received the M.Eng. (Hons.) and Ph.D. in electronic and communications engineering from The University of Sheffield, Sheffield, U.K., in 2015 and 2019, respectively. He joined the University of Sheffield as a Research Associate in 2019, and became an Academic Fellow in 2020. His current research interests include energy efficient radio transmitters and receivers, reconfigurable antennas and metamaterials, and their applications in wireless communications systems.

Timothy O'Farrell (M'91–SM'18) received a B.Sc. (Hons.) degree from the University of Birmingham, U.K., and M.Sc. (Distinction) and Ph.D. degrees from the University of Manchester, U.K. all in Electrical and Electronics Engineering. He is Chair Professor in Wireless Communications at the University of Sheffield, U.K., where he specializes in direct digitization for software defined radios, waveform design for wireless communications, and energy efficiency in mobile radio access networks. He has published extensively on these topics with over 335 journal and conference papers, book chapters, patents and technical reports for industry. He has an established record of research leadership having led 24 major research projects as PI for EPSRC, NERC, EU, DSTL and industry. He was the Academic Coordinator of the Core 5 Green Radio project (2009-2012) and a leader in establishing energy efficiency in wireless networks as a global research field. His current grant portfolio includes Direct Digitisation for Frequency Agile Millimetre Wave Massive MIMO (EP/S008101/1) and Next Generation Information Networks (DSTL). His recent grant portfolio includes the UK Research Strategy Community Organisation in Communications, Mobile Computing and Networking (EP/N007824/1), Frequency Agile Radio (EP/M013723/1), Seamless and Adaptive Wireless Access for Efficient Future Networks (EP/L026147/1) and Networks of Sensors in Extreme Environments (NE/I007148/1). Professor O'Farrell was co-founder and CTO of Supergold Communication Limited (1997-2007), a start-up company founded on his waveform research, which contributed to the IEEE802.11g WiFi standard. He has chaired numerous tracks and workshops in IEEE ICC, VTC and PIMRC and in 2018 he was General Chair of the 5th International Workshop on Next Generation Green Wireless Networks (Next-GWiN 2018). He is a member of the DCMS College of Experts (gov.uk/dcms), a member of the UK5G Climate and Environment Working Group (uk5g.org) and a Director of the mVCE. He is a Chartered Engineer, an IET member and an IEEE senior member.

Mohammad Reza Anbiyaei received his M.Sc. (with distinction) and Ph.D. degrees from the Electronic and Electrical Engineering Department of the University of Sheffield in 2012 and 2018, respectively, where he was a research associate from April 2018 to March 2019. He is currently a postdoctoral research fellow with the Faculty of Engineering, Alzahra University, Tehran, Iran. His research interests include anomaly detection of communication systems using machine learning and artificial intelligence; software-defined radio; reconfigurable, concurrent multiband transceivers; and array signal processing.

Kenneth Lee Ford (Senior Member, IEEE) received the B.Eng. and Ph.D. degrees in electronic engineering from The University of Sheffield, Sheffield, U.K. in 1998 and 2003, respectively. In 2001, he joined the Stealth Materials Department, Advanced Technology Center, BAE Systems, Towcester, U.K. In 2005, he joined The University of Sheffield, as a Lecturer of communications, and then became a Senior Lecturer in 2012. His current research interests include reconfigurable antennas, miniaturized antennas, metamaterials, propagation in the built environment, and electromagnetic structures for biomedical applications.